Measurement of the ^{24}Mg(^{3}He, p)^{26}Al cross section: Implication for ^{26}Al production in the early solar system

C. Fitoussi,[1,*] J. Duprat,[1] V. Tatischeff,[1] J. Kiener,[1] F. Naulin,[1] G. Raisbeck,[1] M. Assunção,[1] C. Bourgeois,[2] M. Chabot,[2] A. Coc,[1] C. Engrand,[1] M. Gounelle,[1] F. Hammache,[2] A. Lefebvre,[1] M.-G. Porquet,[1] J.-A. Scarpaci,[2] N. de Séréville,[2] J.-P. Thibaud,[1] and F. Yiou[1]

[1]*CSNSM (Centre de Spectrométrie Nucléaire et de Spectrométrie de Masse), UMR IN2P3/CNRS and Université Paris-Sud 11, F-91405 Orsay Cedex, France*

[2]*IPNO (Institut de Physique Nucléaire d'Orsay), IN2P3/CNRS and Université Paris-Sud 11, F-91406 Orsay Cedex, France*

(Received 22 June 2008; published 16 October 2008)

The nucleosynthetic origin of ^{26}Al ($t_{1/2} = 0.72$ Myr) in the early solar system is still an open question. Several models predict that short-lived radionuclides could be produced by irradiation of circumsolar material by light charged particles emitted by the young sun. Within some models, most of the ^{26}Al is produced by ^{3}He-induced reactions on ^{24}Mg. Little experimental data exist on ^{3}He reactions so that irradiation models have had to rely on theoretical cross sections deduced from statistical nuclear reaction codes. We performed a direct measurement of the ^{26}Al production on Mg target by means of γ ray spectroscopy and accelerator mass spectrometry (AMS). The data indicate that the theoretical cross section used in previous approaches was overestimated by a factor of 3. Taking the particle spectra considered in theoretical approaches these data lead to a net reduction of the ^{26}Al production of a factor of 2. We calculated the relative contribution of the different ^{26}Al production channels depending on the irradiation scenario. We show that extremely large particles fluxes would be necessary to reach the canonical ^{26}Al/^{27}Al $= 5 \times 10^{-5}$ in solids that were present in the early solar system. An *in situ* origin of this important isotopic chronometer by irradiation is unlikely.

DOI: 10.1103/PhysRevC.78.044613 PACS number(s): 25.55.−e, 25.20.Lj, 96.10.+i

I. INTRODUCTION

From the linear correlation between ^{26}Mg excess and ^{27}Al content in calcium-aluminum-rich inclusions (CAIs) of Allende carbonaceous chondrite, Lee *et al*. 1976 [1] deduced a ratio ^{26}Al/^{27}Al $= 5 \times 10^{-5}$ in the early solar system at the time of isotopic closure of their mineral phases. Since this pioneering work, ^{26}Mg excesses have been reported in a large set of CAIs and in a few chondrules with highest values confirming this initial ratio that hereafter will be referred as the canonical value (e.g., [2,3]). We note that recent data by Young *et al*. suggest an initial "supra-canonical value" 25% higher than the canonical one [4]. CAIs and chondrules are thought to be among the first phases that condensed in the early solar system. Absolute Pb-Pb ages of these refractory phases are found ranging from (4567.2 ± 0.6) Myr to (4564.7 ± 0.6) Myr [5]. Moreover, there is numerous experimental evidence that other radioactive nuclei with half-lives in the Myr range were present in the early solar system [6,7]. For some of these short-lived radionuclides (such as ^{26}Al,^{41}Ca,^{10}Be,^{60}Fe), their inferred concentration in the early solar system is found to be well above the expected value from the chemical evolution of the galaxy [8], indicating that nucleosynthetic events occurred on a Myr time scale before or during the solar system formation.

The first hypothesis is a stellar origin of these nuclei (e.g., [9] for a review). Various types of stars have been considered, including Wolf-Rayet [10], Asymptotic Giant Branch [6,11], and type II Supernovae [12]. Excesses of ^{60}Ni correlating with ^{56}Fe/^{58}Ni reported both in Fe-Sulphids of Chervony Kut eucrite and in the Semarkona ordinary chondrite indicate a ^{60}Fe/^{56}Fe ratio of 7.3×10^{-7} in the early solar system [13]. Large ^{60}Fe/^{56}Fe ratios are expected in massive stars nucleosynthesis [15,16]. By contrast ^{60}Fe cannot be produced by alternative scenarios such as irradiation of circumsolar material in the early solar system [17] because of the lack of abundant stable targets. Although the actual initial ^{60}Fe/^{56}Fe ratio is still debated ^{60}Fe plays the role of the smoking gun for the seeding of the young solar system by at least one last-minute stellar nucleosynthetic event. Even though ^{26}Al can be produced at a satisfactory level by numerous stellar models, up to now none of them could reproduce the global pattern of all the observed short-lived nuclei [6].

An alternative explanation proposed for the production of at least some of the short-lived nuclei (^{10}Be, ^{26}Al, ^{36}Cl, ^{41}Ca) is that solar system material may have undergone nonthermic nucleosynthesis during an early active phase of the sun. Since the first work by Fowler *et al*. 1962 [18], this hypothesis has been regularly discussed (see [17,19–21]). X-ray data from young stellar objects (YSO) suggest that the young sun could have gone through an active phase in which circumstellar matter could have been irradiated by light charged particles [22]. Classical irradiation scenarios have been proposed considering the interaction at asteroidal distance of solar energetic particles (SEP) (p and ^{4}He) with targets of solar compositions. As a general feature, the conventional irradiation scenarios fail to reproduce the measured abundance of ^{26}Al and a general conclusion of these approaches is that the ^{26}Al observed in

*Present address: ETH Zürich, IGMR, Clausiusstrasse 25, 8092 Zürich, Switzerland.

CAIs rather results from a last-minute stellar nucleosynthesis [19].

Aiming at proposing a theoretical approach to understand the physical structures observed in young stellar objects and an astrophysical theory of CAIs and chondrules, Shu *et al.* proposed the so-called *x-wind model* [23,24]. Within the framework of this model, Lee *et al.* [17] proposed an alternative irradiation approach in which they calculated the relative production by irradiation of several short-lived nuclei such as ^{26}Al, ^{41}Ca, ^{53}Mn, ^{138}La. The approach presented in [17] noticeably differs from classical irradiation scenarios on several points. The irradiation occurs at very close distance from the young star (0.06 AU), in the reconnection ring, which is constantly fed by rocks from the accretion disk [17]. A key feature of this scenario is that the authors considered the possibility of large ^{3}He excess in the irradiating flux, by analogy with impulsive flares occurring in reconnection events observed in the modern sun [25]. In [17], in order to reproduce the canonical ^{26}Al/^{27}Al ratio, the authors considered an unusually high ^{3}He/^{4}He = 14, well above the average values (0.1–1) reported in impulsive flares [25–27]. Under these conditions the main reaction involved in the ^{26}Al production is ^{24}Mg(^{3}He, p)^{26}Al. The authors of [17] emphasized that such a high ^{3}He component induces a major collateral production of ^{41}Ca through the ^{40}Ca(^{3}He, 2p)^{41}Ca reaction that overproduces ^{41}Ca by about 2 orders of magnitude compared to the ^{41}Ca/^{40}Ca = 1.5×10^{-8} reported for CAIs [28,29]. To cope with this issue, Gounelle *et al.* [21,30] proposed a model in which the relative abundances of several short-lived nuclei (^{26}Al, ^{41}Ca, ^{53}Mn, ^{138}La), including the ^{10}Be/^{9}Be ratio reported in Allende CAIs by McKeegan *et al.* [31], could be reproduced [21,30].

In these approaches, ^{3}He plays a crucial role for ^{26}Al production but very little experimental data exists on absolute ^{3}He-induced cross sections. In both [17,21] and [30] the main ^{26}Al production channel is ^{24}Mg(^{3}He, p)^{26}Al for which they used a numerical simulation performed with the PACE code [32]. Betts *et al.* [33] studied the nuclear structure of ^{26}Al by means of the ^{24}Mg(^{3}He, p)^{26}Al reaction at an incident energy of 18 MeV. They reported the angular distribution of the proton spectra of the 65 first levels. Using the data from [33] and the branching ratios from [34], we summed all levels decaying to the 5^{+} ground state of ^{26}Al and obtained a value of 8.2 mb for the total population of the ground state at 18 MeV. In the Hauser-Feshbach approach used in [17], the estimated cross section is 50 mb at the same incident energy (see Fig. 3 in [17]); that is, a discrepancy of a factor of 6. Still, the extrapolation of the cross section from 18 MeV to the energy range of interest where the cross section is maximum (between 3 to 15 MeV) is not trival since the value at 18 MeV is already a factor of 10 lower than the the maximum value expected at about 7 MeV.

The aim of the present paper is to present experimental data on ^{26}Al production by ^{3}He-induced reactions on Mg targets over the full energy range of interest, from 3 MeV up to 30 MeV (see Fig. 3 in [17]).

II. EXPERIMENTAL SETUP

The experiment was performed in two steps. A first part took place at the 14MV Tandem accelerator of IPN-Orsay where targets of ^{24}Mg and natural Mg (^{nat}Mg) were irradiated and the cross section measured via the detection of ^{26}Al γ-rays. This irradiation was part of an experiment to study ^{3}He-induced cross sections relevant to γ-ray line emission in solar flares [35]. Since a part of the total ^{26}Al^{g} ground state (5^{+}, $t_{1/2}$ = 0.72 Myr) production occurs through direct population of the 5^{+} state with no γ-ray emission, we also irradiated a set of targets and analyzed the resulting ^{26}Al content by means of Accelerator Mass Spectroscopy (AMS) at the Tandetron of Gif-sur-Yvette [36].

We restricted the γ-ray analysis to the 417 keV transition connecting the second excited state (3^{+}) to the ground state (5^{+}). We used this γ-ray to extrapolate the ^{24}Mg(^{3}He, p)^{26}Al^{g} cross section below 6 MeV (where we had no AMS data, see discussion in Sec. II A). We also used the 417 keV transition recorded on natural Mg targets, that is ^{nat}Mg(^{3}He, $\gamma_{417\,\mathrm{keV}}x$)^{26}Al^{g}, to deduce the relative contribution of the two minor isotopes ^{25}Mg and ^{26}Mg.

A. The Tandem experiment

The ^{3}He beam was delivered in a 2+ charge state by the Tandem accelerator with energies ranging from 3 up to 36 MeV. We used self-supported ^{24}Mg and ^{nat}Mg targets. The thicknesses of the targets ranged from 0.5 to 17.7 mg/cm^{2}. All ^{24}Mg targets were enriched >99%. Due to the large number of targets and the numerous energies studied, a ten position multiple target holder was used in order to quickly change targets in the chamber for each beam energy. The reaction chamber was equipped with an optical window and an external video to control the beam size and position with an alumina foil located at the middle position of the target holder. The beam size was 1–2 mm^{2} while the target size was about 1 cm^{2}. The outgoing ^{3}He^{2+} beam was measured in a Faraday cup with an entrance located 1.4 m behind the target. The Faraday cup consisted of a 1.5 m long tube equipped with an electron repelling ring ($V = -400$V) located at the entrance of the tube. The current measured at the end of the tube was integrated in a Digital Current Integrator (ORTEC 439). The current delivered to the targets ranged from 5 to 20 nA.

The γ-rays were detected with four large volume high purity germanium (Ge) detectors located at 37 cm from the target and $\theta_{\mathrm{lab}} = 90^{\circ}$, 112.5°, 135°, and 157.5° with respect to the beam direction. The Ge crystals were surrounded by bismuth germanate (BGO) detectors for Compton suppression [37]. The experimental setup is shown on Fig. 1. The detectors efficiencies were determined using calibrated radioactive sources (^{60}Co, ^{88}Y, ^{137}Cs, ^{152}Eu) and proton-induced reactions for which γ-production cross sections are known: ^{24}Mg(p, p')^{24}Mg (E_{γ} = 1.37 MeV) and ^{16}O(p, p')^{16}O (E_{γ} = 2.74 and 6.13 MeV). The overall dead time was monitored for each run by feeding the preamplifiers of the Ge detectors with pulsers of known frequency (100 Hz). The dead time correction was inferred by measuring the ratio between the intensity of the pulser lines observed in the Ge spectra and the known number of pulses that was sent to each detector during the run. The acquisition system also provided a dead time measurement by measuring the amount of time when the system was busy. The

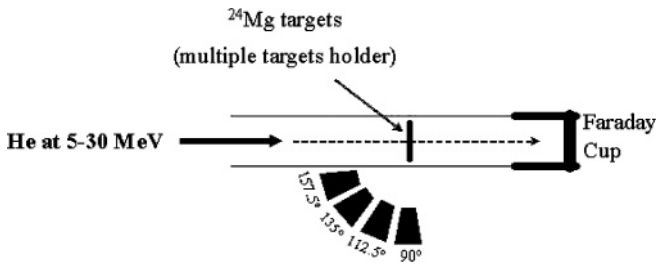

FIG. 1. Schematic view of the Tandem Experiment.

two dead times were found to be similar and the uncertainty on the dead time was 3%. The dead time was found to range from 15% to 40% for the thin target (5 mg/cm^2) and from 50% to 60% for the thicker targets.

B. The AMS experiment

In order to have access to the total cross section, we irradiated with ^{3}He beam 11 ^{24}Mg targets, of thicknesses ranging from 0.5 up to 17.7 mg/cm^2 as a compromise between ^{26}Al production and beam straggling and energy losses. After irradiation, the targets were left apart for two years for short-period nuclei radioactive decay (the activity was essentially coming from ^{22}Na, $t_{1/2} = 2.603$ yr). Each target was cut out from the target holder with a stainless steel scalpel, and washed with acetone. In a 50 mL centrifuged tube, 1 mL of ^{27}Al carrier (10^{-3}g/mL) was added to each sample. A few mL of HCl 3N were used to dissolve the targets. When the dissolution was completed, the pH of the solution was adjusted to 8 with NH_{3aq} to form $Al(OH)_3$ precipitate. The pH should not be too much higher to avoid large $Mg(OH)_2$ precipitation. The aluminum precipitate was centrifuged 10 min at 3500 rpm, the aqueous phase was discarded, the precipitate was rinsed with Millipore ultrapure water (UPW) adjusted at pH = 8 with NH_{3aq}. The last step was repeated twice. The precipitate was dissolved with 400 μL of HNO_3(12%) and transferred into a quartz crucible. The centrifuged tube was rinsed twice with 200 μL HNO_3 (12%) + 200 μL UPW at pH = 8. The solution was evaporated to dryness on a hotplate, then heated up at maximum hotplate temperature for 30 min, and oxydized to Al_2O_3 in an electrical furnace at 900°C for 45 min. The Al_2O_3 powder was pressed into a molybdenum cathode. Blank samples were prepared from unirradiated ^{24}Mg targets following the same chemical procedure.

The AMS measurements were performed at the Tandetron facility of Gif-sur-Yvette. These were the first measurements of ^{26}Al/^{27}Al ratios performed on the heavy ion line [36]. Al was injected in the ion source as Al^- so that there was no isobaric interference injected with ^{26}Mg, as $^{26}Mg^-$ is not stable. Measurement efficiency was determined using two standard runs, one preceding and one following sample analyses. Two blanks were measured. The sample ratios were calculated by subtracting the average number of ^{26}Al atoms in the blanks from that of the targets.

The sample ^{26}Al/^{27}Al ratio ranged from 3×10^{-12} up to 3×10^{-10}, leading to measurements well above the measured blank level with $R_{blank} = 1.48 \times 10^{-13}$. As mentioned above, the targets used as blanks were ^{24}Mg targets, identical to the ones used to measure the cross section, but not irradiated; however, they were stored in the room dedicated to irradiated targets, which might explain why the blank ratio is higher than our usual ^{26}Al AMS blank by more than an order of magnitude.

C. Data analysis and results

The data analysis can be separated in two distinct phases. The γ-ray data are used to infer both the low energy part of the $^{26}Al^g$ total production and the contribution of the minor ^{25}Mg and ^{26}Mg isotopes, while the AMS data provides the ^{24}Mg(^{3}He, p)$^{26}Al^g$ production between 6 and 25 MeV.

1. Gamma ray data

The raw data were sorted using the OASIS offline software [38]. We constructed a γ-ray energy spectrum for each of the four Ge detectors and for each ^{3}He incident energy. Examples of such a spectrum are displayed in Fig. 2 for ^{24}Mg targets at 6 MeV and 15 MeV incident energy. The main exit channels are (^{3}He, p)^{26}Al, (^{3}He, $2p$)^{25}Mg for ^{3}He energies below 10 MeV. For higher energies the $2pn, \alpha, \alpha p$, and αpn are slowly taking over. For all energies the strongest γ rays observed are the 1368 keV line from ^{24}Mg excitation and the 511 keV (e^+e^-) recombination line from β^+ decay within the target. We applied the same procedure on natural Mg targets (Fig. 3).

A partial level scheme of $A = 26$ is indicated in Fig. 4, where we report the main γ-transitions seen during the experiment. The indirect contribution of ^{24}Mg(^{3}He, n)^{26}Si $\rightarrow^{26}$ Al can be neglected for the analysis of both the 417 keV γ-ray intensity and the final 5^+ state population. The (^{3}He, n) channel represents less than 13% of the (^{3}He, p) channel and 97% of the ^{26}Si population decays through electronic capture to the 1^+ and 0^+ in ^{26}Al, and is thus not contributing to the 3^+ nor the 5^+ state of interest but is decaying rapidly ($t_{1/2} = 6.34$ s) to ^{26}Mg. Finally, all levels above the 3^+ state (1.25 ns) have half-lives below a few picoseconds so that full γ decay of all states of ^{26}Al is taking place within a cm from the target and is thus fully recorded by the Ge detectors. The same will not hold for the long-lived 5^+ state measured by AMS for which the number of $^{26}Al^g$ recoil nuclei escaping from the target must be evaluated (see below).

Using the TRIM code [39], we calculated the averaged energy loss in the target, δE, depending on the incident ^{3}He beam energy (E_b) and on the thickness of the target. The relative uncertainty on the incident energy delivered by the Orsay Tandem is of the order of 10^{-4}, far below the δE values. The effective energy for the cross section measurement reported in all figures and tables was taken as $E = E_b - \delta E/2$ with the uncertainty $\pm\delta E/2$.

We measured the yields by integration of the peaks and subtraction of the background from a linear interpolation on neighboring channels. The 417 keV line was found to be free of contamination at all energies for both ^{24}Mg and ^{nat}Mg targets.

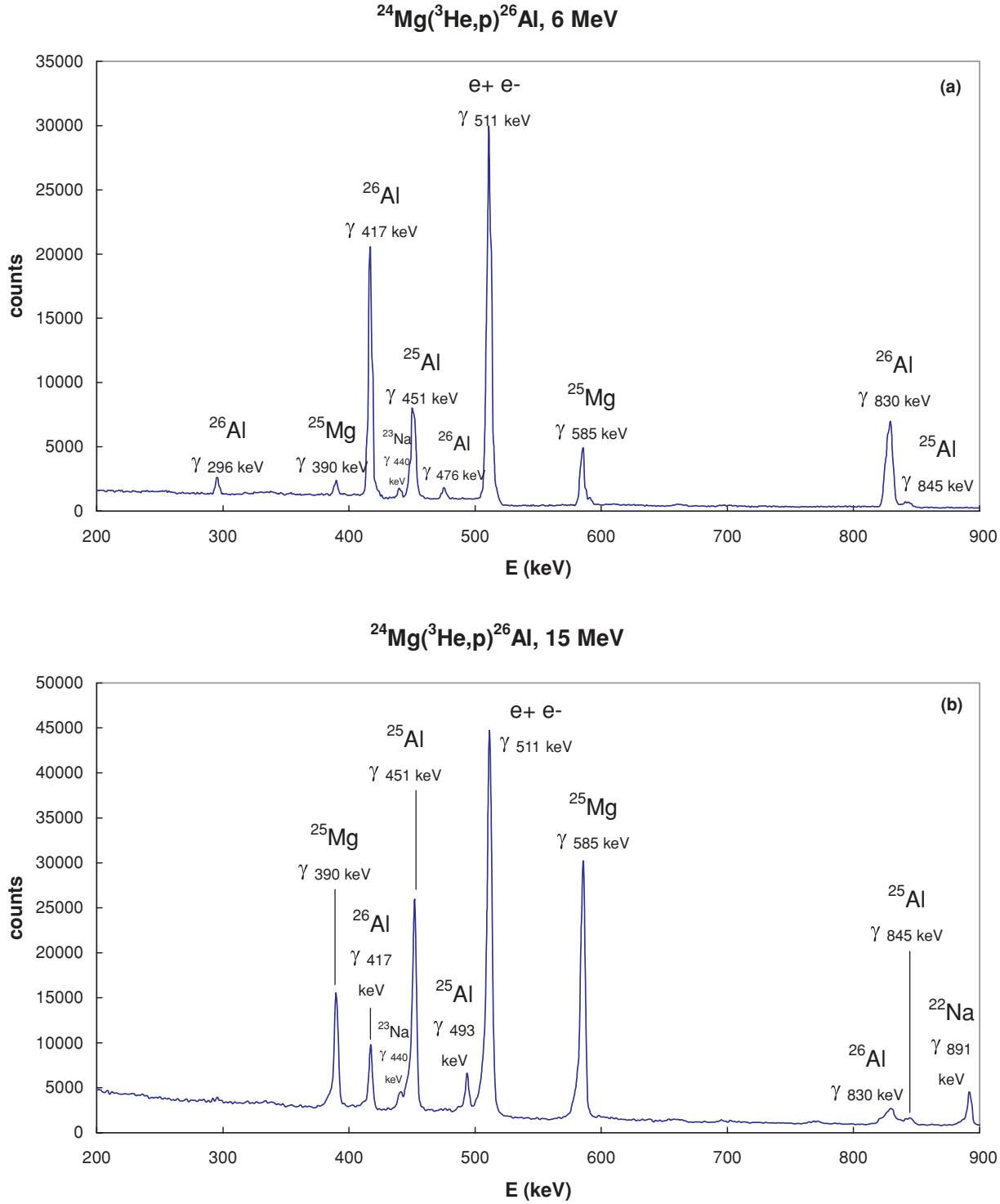

FIG. 2. (Color online) Gamma-ray spectra (a) at 6 MeV of a 0.50 mg/cm^2 ^{24}Mg target (detector at $\theta = 112.5^\circ$); (b) at 15 MeV of a 5.77 mg/cm^2 ^{24}Mg target (detector at $\theta = 135^\circ$).

We computed the differential cross sections (in mb) as

$$\frac{d\sigma_{\mathrm{Gei}}}{d\Omega(\theta_{\mathrm{lab}})} = \frac{N_{\mathrm{Gei}}}{(\varepsilon_{\mathrm{Gei}} \times (Q \times 10^{-10}/2e) \times (1 - t_{\mathrm{deadtime}}) \times T \times 10^{-3}/24.305 \times N)} \times 10^{27},$$

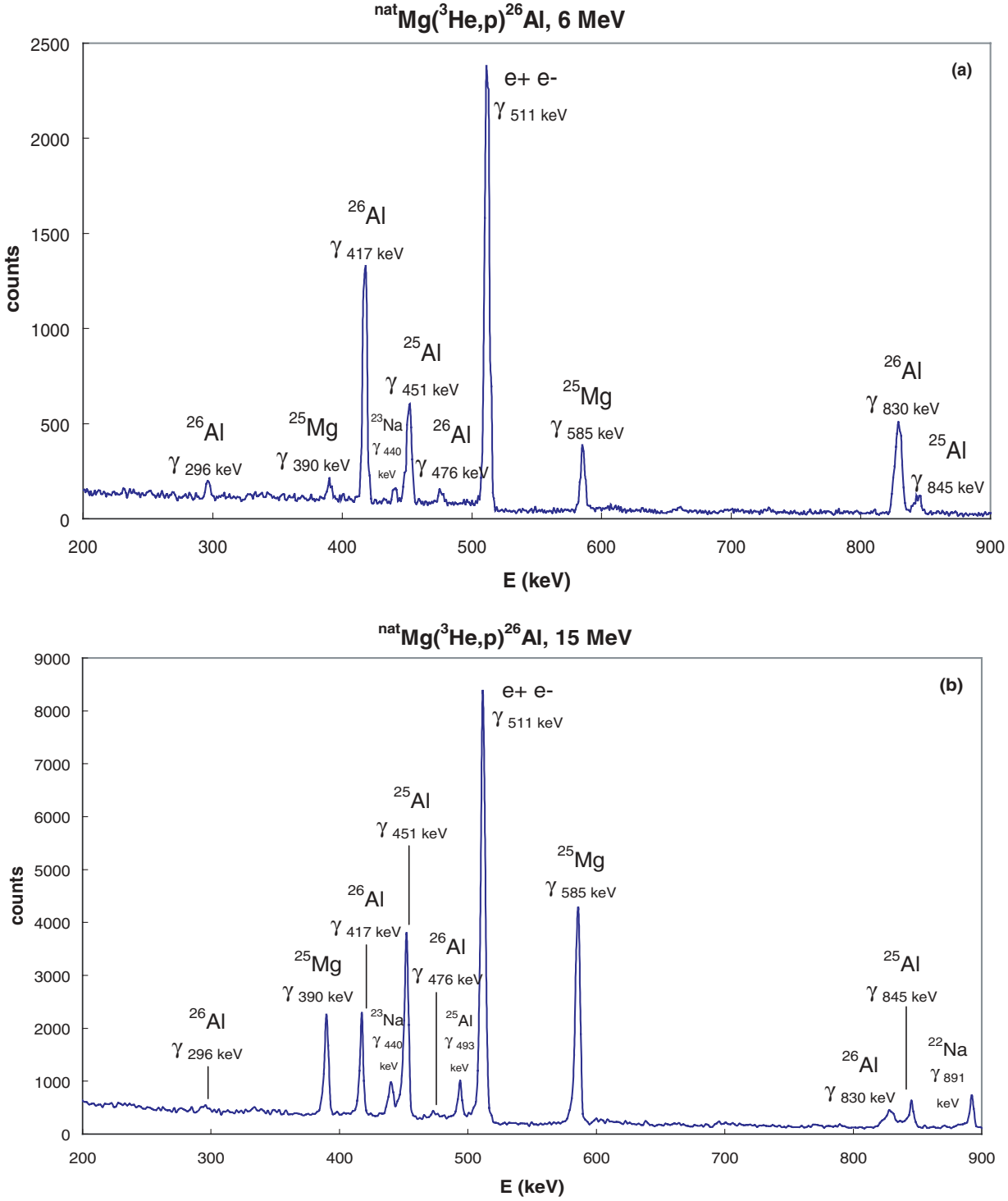

FIG. 3. (Color online) Gamma-ray spectra (a) at 6 MeV of a 0.33 mg/cm^2 $^{\text{nat}}$Mg target (detector at $\theta = 112.5^\circ$); (b) at 15 MeV of a 1.44 mg/cm^2 $^{\text{nat}}$Mg target (detector at $\theta = 135^\circ$).

that is

$$\frac{d\sigma_{\text{Gei}}}{d\Omega(\theta_{\text{lab}})} = 0.1293 \times \frac{N_{\text{Gei}}}{(\varepsilon_{\text{Gei}} \times Q \times (1 - t_{\text{deadtime}}) \times T)},$$

where N_{Gei} is the number of counts in the detector Ge$_i$, ε_{Gei} is the efficiency of the Ge detector, Q (in 10^{-10} C) is the total charge deposited in the Faraday cup during the irradiation of the ^{24}Mg target with ^{3}He^{2+}, T (in mg/cm^2) the thickness, e the electron charge, N Avogadro's number.

The uncertainty in dσ/dΩ, for each detector takes into account the error on target thickness (10%), the error on Q(5%), the dead time correction (3%).

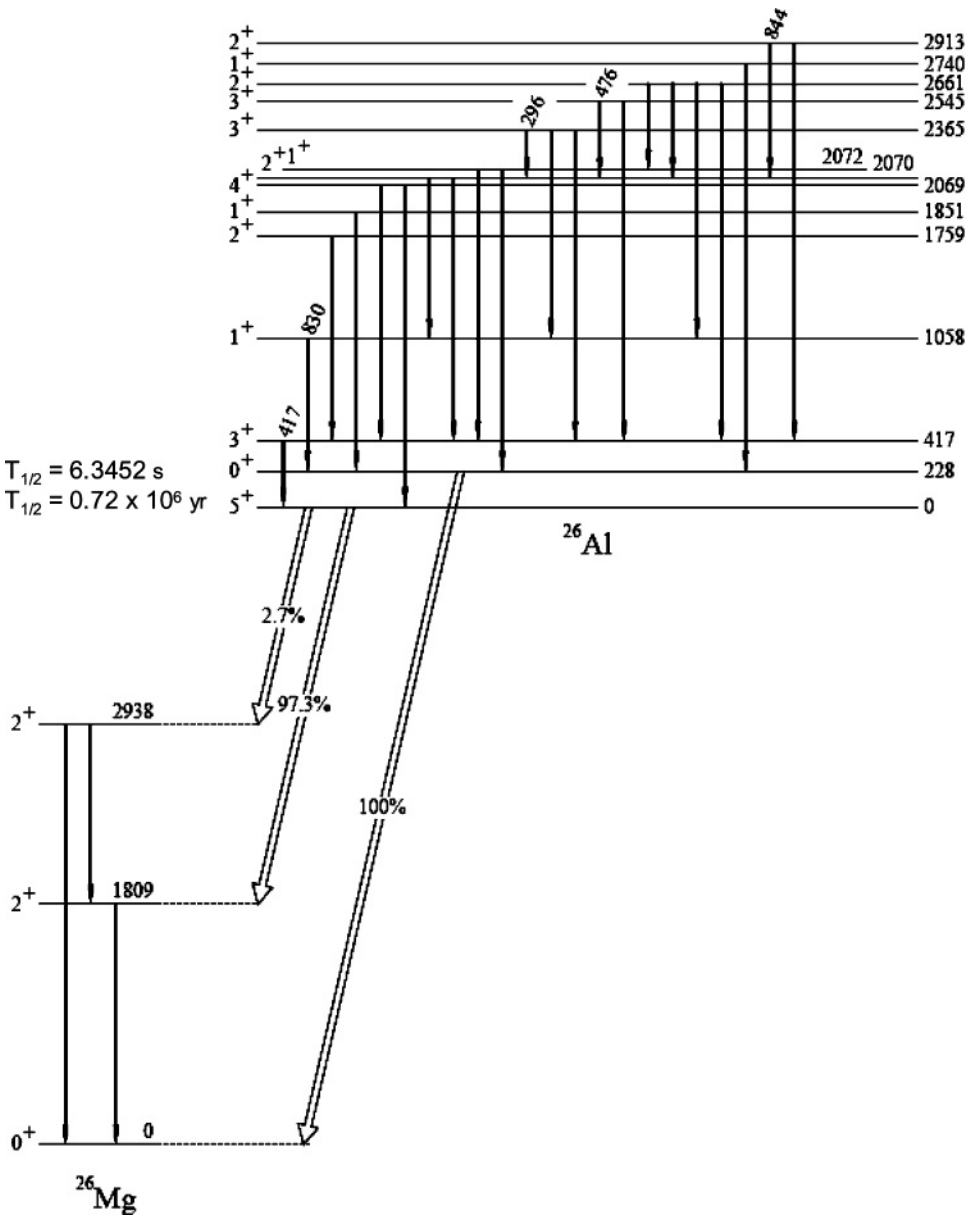

FIG. 4. Partial energy levels scheme of nuclei produced in ^{3}He + ^{24}Mg reactions, giving γ transitions of interest.

The angular dependence of the 417 keV line was fitted as

$$d\sigma/d\Omega(\theta_{\rm lab}) = a_0 + a_2 C_2 P_2(\cos\theta_{\rm lab}) + a_4 C_4 P_4(\cos\theta_{\rm lab}),$$

where the $P_\ell(\cos\theta_{\rm lab})$ are the Legendre polynomial of order ℓ and Ci the attenuation coefficients which have been analytically calculated from the experimental setup geometry [40]. The total cross section is given as

$$\sigma = 4\pi a_0.$$

We report the total cross sections for the 417 keV emission on Fig. 5 for the ^{24}Mg targets. One data point at 14.3 MeV gives a cross section below those obtained from the rest of the measurements in the same energy range for a nonunderstood reason. The total cross sections for the 417 keV for the $^{\rm nat}$Mg targets are shown on Fig. 6. The corresponding values are reported in Tables I and II, respectively.

2. AMS data

The total 5^+ production was deduced from AMS measurements on a set of ^{24}Mg targets reported in Table III. For each ^{3}He bombarding energy, we computed the total cross section as

$$\sigma = \frac{[^{26}\mathrm{Al}] \times F_{\rm esc}}{((Q \times 10^{-10}/2e) \times T \times 10^{-3}/24.305 \times N)} \times 10^{27},$$

$$\sigma = 0.1293 \times {}^{26}\mathrm{Al}\, N_{\rm AMS} \times F_{\rm esc}/(Q \times T),$$

where $[^{26}\mathrm{Al}]$ $^{26}\mathrm{Al}\, N_{\rm AMS}$ is the number of ^{26}Al atoms in the target deduced from the AMS measurement and $F_{\rm esc}$ the factor accounting for the escape of the recoiling nuclei in the target (see below). Q (in 10^{-10} C) the charge measured during the irradiation of the ^{24}Mg target with ^{3}He^{2+}, T (in mg/cm^2) the thickness of the target, e the electron charge, N Avogadro's number.

TABLE I. Cross section for the production of the 417 keV γ-ray line via the reaction ^{24}Mg(^{3}He, $p\gamma_{417\,\mathrm{keV}}$)^{26}Al.

E(MeV)	T(mg/cm^2)	σ(mb)
3.1 ± 0.6	1.88	4.4 ± 0.4
3.5 ± 0.2	0.56	6.9 ± 0.7
3.8 ± 0.2	0.56	14 ± 1
4.1 ± 0.2	0.56	24 ± 2
4.3 ± 0.2	0.56	35 ± 3
4.6 ± 0.2	0.56	43 ± 4
4.9 ± 0.2	0.56	57 ± 6
5.1 ± 0.1	0.56	59 ± 6
5.4 ± 0.1	0.56	68 ± 7
5.6 ± 0.1	0.56	85 ± 8
5.9 ± 0.1	0.50	87 ± 8
6.1 ± 0.1	0.56	93 ± 9
6.4 ± 0.1	0.56	100 ± 10
6.6 ± 0.1	0.56	101 ± 10
6.9 ± 0.1	1.88	93 ± 9
7.1 ± 0.1	0.56	95 ± 9
7.4 ± 0.1	0.56	100 ± 10
7.6 ± 0.6	3.40	91 ± 9
7.6 ± 0.1	0.56	96 ± 9
7.9 ± 0.4	1.88	97 ± 9
8.2 ± 0.1	0.56	92 ± 9
8.4 ± 0.1	0.56	91 ± 9
8.7 ± 0.1	0.56	88 ± 9
8.7 ± 0.3	1.88	79 ± 8
8.9 ± 0.7	4.12	76 ± 7
9.2 ± 0.1	0.56	77 ± 7
9.4 ± 0.1	0.56	74 ± 7
9.4 ± 0.3	1.88	72 ± 7
9.7 ± 0.1	0.56	69 ± 7
10.2 ± 0.1	0.56	65 ± 6
10.2 ± 0.6	3.93	56 ± 5
10.4 ± 0.4	2.38	53 ± 5
11.2 ± 0.4	2.38	49 ± 5
11.7 ± 0.3	2.38	45 ± 4
11.9 ± 0.6	4.27	36 ± 3
12.2 ± 0.3	2.38	44 ± 4
12.7 ± 0.3	2.38	42 ± 4
13.2 ± 0.3	2.38	38 ± 4
13.7 ± 0.3	2.38	34 ± 3
14.2 ± 0.3	2.38	27 ± 3
14.3 ± 0.7	5.77	14 ± 1
14.7 ± 0.3	2.38	26 ± 3
19.8 ± 0.2	2.38	10 ± 1
24.8 ± 0.2	2.38	4.9 ± 0.5
29.8 ± 0.2	2.38	3.9 ± 0.4
35.9 ± 0.2	2.38	1.7 ± 0.2

TABLE II. Cross section for the production of the 417 keV γ-ray line via the reaction $^{\mathrm{nat}}$Mg(^{3}He, $p\,\gamma_{417\,\mathrm{keV}}$)^{26}Al.

E (MeV)	T(mg/cm^2)	σ(mb)
3.6 ± 0.1	0.33	7 ± 1
3.9 ± 0.1	0.33	14 ± 1
4.2 ± 0.1	0.33	22 ± 2
4.4 ± 0.1	0.33	31 ± 3
4.7 ± 0.1	0.33	39 ± 4
4.9 ± 0.1	0.33	48 ± 5
5.2 ± 0.1	0.33	51 ± 5
5.4 ± 0.1	0.33	65 ± 6
5.7 ± 0.1	0.33	73 ± 7
5.9 ± 0.1	0.33	84 ± 8
6.2 ± 0.1	0.33	85 ± 8
6.4 ± 0.1	0.33	89 ± 9
6.7 ± 0.1	0.33	93 ± 9
7.2 ± 0.1	0.33	88 ± 9
7.4 ± 0.1	0.33	86 ± 8
7.7 ± 0.1	0.33	86 ± 8
8.2 ± 0.1	0.33	82 ± 8
8.4 ± 0.1	0.33	84 ± 8
8.7 ± 0.1	0.33	82 ± 8
9.2 ± 0.1	0.33	78 ± 8
9.7 ± 0.1	0.33	75 ± 7
10.2 ± 0.1	0.33	65 ± 6
10.6 ± 0.1	1.44	62 ± 6
10.8 ± 0.1	1.44	54 ± 5
11.3 ± 0.1	1.44	50 ± 5
11.8 ± 0.1	1.44	51 ± 5
12.3 ± 0.1	1.44	53 ± 5
12.8 ± 0.0	1.44	53 ± 5
13.3 ± 0.0	1.44	49 ± 5
13.8 ± 0.0	1.44	46 ± 5
14.3 ± 0.0	1.44	41 ± 4
14.8 ± 0.0	1.44	39 ± 4
19.9 ± 0.0	1.44	24 ± 2
24.9 ± 0.0	1.44	16 ± 2
29.9 ± 0.0	1.44	15 ± 1
35.9 ± 0.0	1.44	12 ± 1

By contrast with the prompt γ-ray data, the AMS results have to be corrected for potential escape of the recoiling ^{26}Al from the target. We performed therefore detailed simulations of the recoil of ^{26}Al and its slowing down in the target in a Monte Carlo type approach. The recoil energies and angles were calculated from the differential cross sections and excitation energy distributions of the (^{3}He, p) reaction, which we obtained from the TALYS reaction code at each indident energy. We used the SRIM software package for the stopping calculations of the recoiling ^{26}Al ions.

For each target we performed several simulations by taking three different target thicknesses, the nominal one ($\langle T\rangle$) and the two extremes values of the target uncertainty range ($\langle T\rangle \pm \delta T$). The differences of the escape fraction related to the nuclear reaction parameters (excitation energy distribution, angular distribution) were negligible with respect to the differences which resulted from the target thickness variations. The escape fraction values reported in Table III are obtained using the mean value for the target thickness ($\langle T\rangle$), the $F_{\mathrm{esc}} + \Delta^{+}$and $\mathrm{F_{esc}} - \Delta^{-}$are the ones for $\langle T\rangle + \delta T$ and $\langle T\rangle - \delta T$, respectively.

As one can see in Table III, the correction factors are below 10% for all targets, except for the thinnest targets ($\langle T\rangle = 0.5$ and 1.51 mg/cm^2). We applied these correction factors to the cross section, and the resulting values are reported on Fig. 5 and Table III.

TABLE III. ^{24}Mg(^{3}He, p)^{26}Al^{g} cross section deduced from AMS measurement.

E (MeV)	T(mg/cm^2)	[^{26}Al] (atoms)	σ_{meas}(mb)	F_{esc}	σ_{corr}(mb)
5.9 ± 0.1	0.50 ± 0.05	$1.92 \pm 0.18 \times 10^8$	69 ± 10	$2.13^{+0.60}_{-0.44}$	147^{+47}_{-37}
7.6 ± 0.6	3.40 ± 0.34	$1.98 \pm 0.15 \times 10^9$	141 ± 19	$1.10^{+0.14}_{-0.11}$	155^{+29}_{-26}
8.9 ± 0.7	4.12 ± 0.41	$2.34 \pm 0.18 \times 10^9$	153 ± 21	$1.09^{+0.14}_{-0.11}$	167^{+31}_{-28}
10.2 ± 0.6	3.93 ± 0.39	$1.56 \pm 0.12 \times 10^9$	111 ± 15	$1.10^{+0.14}_{-0.11}$	122^{+23}_{-21}
11.9 ± 0.6	4.27 ± 0.43	$1.96 \pm 0.15 \times 10^9$	88 ± 12	$1.11^{+0.14}_{-0.11}$	98^{+18}_{-16}
14.3 ± 0.7	5.77 ± 0.58	$1.93 \pm 0.15 \times 10^9$	50 ± 7	$1.08^{+0.14}_{-0.10}$	54^{+10}_{-9}
17.4 ± 0.6	5.82 ± 0.58	$1.82 \pm 0.14 \times 10^9$	26 ± 4	$1.09^{+0.14}_{-0.11}$	28^{+5}_{-5}
20.4 ± 0.6	6.09 ± 0.61	$1.82 \pm 0.14 \times 10^9$	21 ± 3	$1.10^{+0.13}_{-0.11}$	23^{+4}_{-4}
23.6 ± 1.4	17.7 ± 1.8	$4.32 \pm 0.36 \times 10^8$	13 ± 2	$1.03^{+0.12}_{-0.10}$	14^{+3}_{-2}
23.8 ± 1.2	14.4 ± 1.4	$8.10 \pm 0.61 \times 10^9$	12 ± 2	$1.04^{+0.12}_{-0.10}$	13^{+2}_{-2}
24.9 ± 0.1	1.51 ± 0.15	$7.96 \pm 0.86 \times 10^7$	12 ± 2	$1.71^{+0.34}_{-0.25}$	20^{+5}_{-4}

The vertical error bar in the cross section includes uncertainties in: target thickness, ^{3}He^{2+} integrated flux in the faraday cup, counting statistics, stability of the AMS (5%), and the uncertainty on the escape correction factor (see Table III). The horizontal error bar represents the energy loss in the target calculated with TRIM [39].

III. DISCUSSION

We first compare the ^{26}Al^{g} production cross section obtained by γ-ray spectroscopy and the AMS data with the predictions of theoretical numerical simulations. We evaluate the contribution of the two other minor isotopes ^{25}Mg and ^{26}Mg to infer the total ^{nat}Mg contribution to ^{26}Al^{g} production. We then discuss the implication of these results on the potential production of ^{26}Al by irradiation in the early solar system.

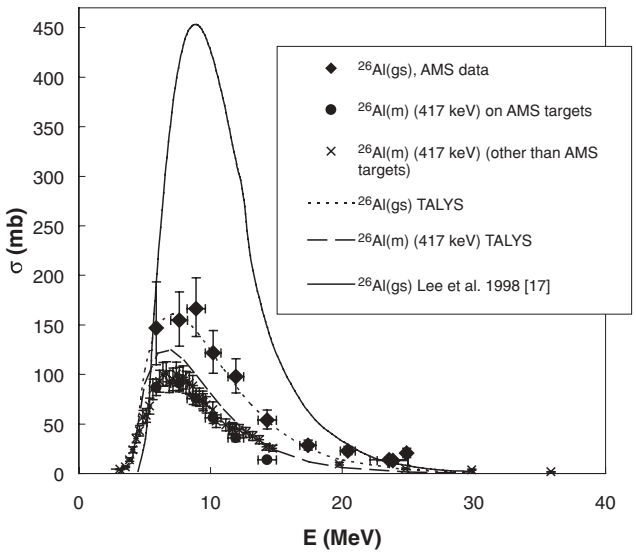

FIG. 5. Comparison of the excited state $(3^+)^{24}$Mg(^{3}He, $p\gamma_{417\,keV}$)^{26}Al$^{(m)}$ cross section deduced from γ-ray data and the ground state (g.s.) ^{24}Mg(^{3}He, p)^{26}Al$^{g.s.}$ cross section deduced from AMS measurement with numerical simulation obtained with TALYS code [41] and from PACE code (from [17]).

A. The ^{24}Mg(^{3}He, p)^{26}Al(5^+, $t_{1/2} = 0.72$ Myr) cross section

In Fig. 5 we compare the experimental data of this work with theoretical expectations. We report the numerical simulations used in [17] and [30] obtained with the PACE code [32]. The excitation function used in both [17] and [30] overestimates the magnitude of the cross section by a factor of 3. In [17], the authors estimate an average uncertainty of about a factor of 2 in their predictions but also mentioned that, especially for channels with $\sigma < 100$ mb, discrepancies up to an order of magnitude can occur between the data and the results from their calculations.

We performed a theoretical calculation using the TALYS code to infer both the 3^+ and 5^+ state populations in ^{26}Al. Taking the default option, the TALYS code reproduces well the absolute magnitude of the ^{26}Al^{g} cross section for energies below 9 MeV but underestimates it by a factor of 2 to 3 for energies from 15 MeV up to 30 MeV (not shown). Since such a discrepancy could arise from a bad approach for the preequilibrium part of the reaction, we checked the different preequilibrium options available in TALYS and noticed that the best fit to the data is provided using the preequilibrium option that calculates the transition rates using an optical model for the collision probability. Still, for energies higher than 20 MeV, we note that the data points are underestimated by a factor 3. Concerning the 417 keV γ-ray intensity, the cross section is overestimated by 25% at maximum and, for $E > 20$ MeV, underestimated by a factor 3. It is interesting to note that the TALYS code reproduces well the data between 3 and 18 MeV, which is the range in energy that really matters for the ^{26}Al production (see below).

For energies below 5 MeV one can see that the simulated population of the 3^+ excited state becomes equal to the simulated total population of the 5^+ ground state. For low

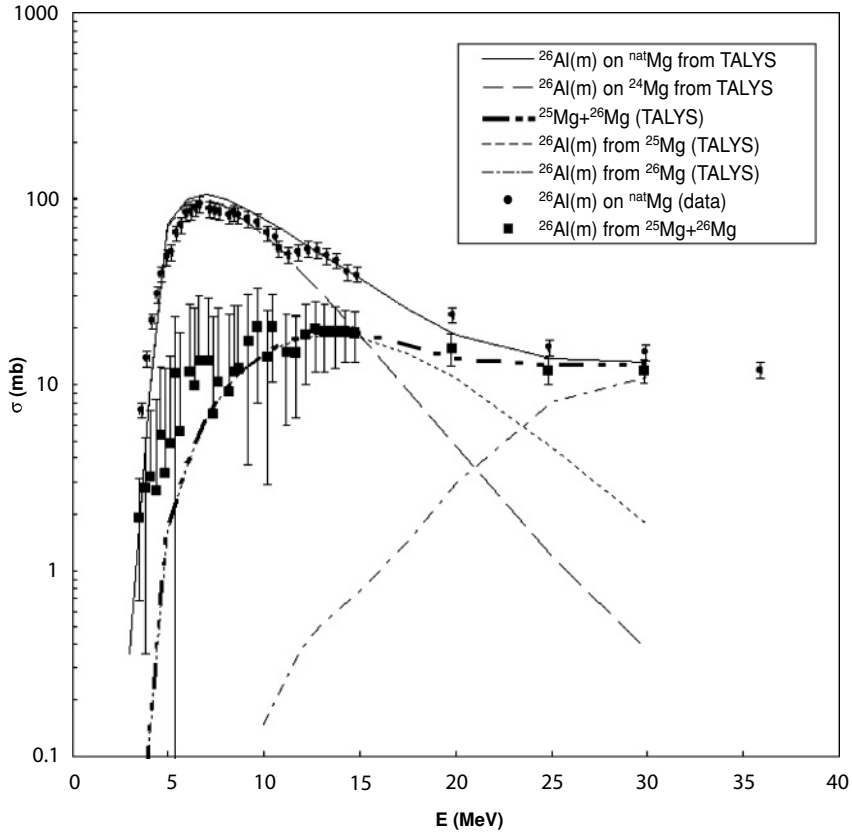

FIG. 6. The ^{25}Mg(^{3}He, $pn\,\gamma_{417\,\mathrm{keV}}$)^{26}Al$^{(m)}$ and ^{26}Mg(^{3}He, $p2n\gamma_{417\,\mathrm{keV}}$)^{26}Al$^{(m)}$ cross section deduced from γ-ray data (417 keV). The black dots are the 417 keV ($3^{+} \rightarrow 5^{+}$) cross section on $^{\mathrm{nat}}$Mg; the black squares are the deduced contribution of the two minor isotopes (^{25}Mg and ^{26}Mg) to this cross section (see text). The lines are the corresponding TALYS calculations.

incident projectile energies, it becomes difficult to directly populate the relatively high spin ($5\hbar$) of the ground state compared to the slightly excited $3\hbar$ state and so the direct population of the ground state is strongly inhibited. In order to evaluate the total ground state cross section at low energy, we extrapolated the low energy part of the cross section by an interpolation between the γ-ray data from 3.5 to 4.5 MeV and the last AMS data point at 6 MeV. The final result is reported on Table I and Fig. 5.

B. The ^{25}Mg and ^{26}Mg contribution

The production of ^{26}Al by ^{3}He induced reactions on $^{\mathrm{nat}}$Mg targets includes a contribution from the two minor isotopes ^{25}Mg (10%) and ^{26}Mg (11%) through ^{26}Mg(^{3}He, $p2n$)^{26}Al and ^{25}Mg(^{3}He, pn)^{26}Al, respectively. We have not performed AMS measurements with $^{\mathrm{nat}}$Mg irradiated targets, but we have recorded γ-ray production on two $^{\mathrm{nat}}$Mg targets (0.33 and 1.44 mg/cm^{2}). The comparison of the 417 keV production on ^{24}Mg with $^{\mathrm{nat}}$Mg provides a possibility to estimate the minor Mg isotopes contribution to ^{26}Al^{g}. The global contribution of ^{25}Mg and ^{26}Mg to the 417 keV line strength $P(417,\ ^{25-26}\mathrm{Mg})$ can be deduced from the subtraction of the two cross sections (see Fig. 6). Even if the resulting data points have large error bars due to the low abundance of Mg minor isotopes, one can see that the contribution of ^{25}Mg and ^{26}Mg starts to be significant only for energies above 10 MeV and then stays below 20 mb on the whole energy range of interest.

In Fig. 6, we also report the theoretical excitation functions of the 417 keV production yield expected in a $^{\mathrm{nat}}$Mg target. These yields were obtained using TALYS code results folded by the relative abundances of the three Mg isotopes. The ^{26}Mg(^{3}He, $p2n$)^{26}Al has a negative Q value (−4 MeV) and its contribution starts for energies above 15 MeV. By contrast, the ^{25}Mg(^{3}He, d)^{26}Al is exothermic ($Q = 0.6$ MeV) and has a contribution for energies from 5 up to 20 MeV. There is a rather good agreement between the theoretical expectation and the experimental data. We note that the ^{24}Mg relative contribution stays superior to 80% for all energies in the 3–10 MeV range where the convolution of the cross section with the ^{3}He spectrum is significant (see below).

C. The ^{26}Al production in the early solar system

The possibility to produce the ^{26}Al/^{27}Al canonical abundance ratio in the early solar system depends on many parameters among which the accelerated particle spectra, the total fluence, the size and composition of the target ([17] and [30]). It also depends on a potential internal structure of the irradiated solids [30]. As a result, the resulting ^{26}Al/^{27}Al in each irradiated solid is expected to exhibit a rather large range of variation mainly depending on its size and irradiation conditions. The mere existence of a "canonical" value for CAIs thus requires a scenario where the solids are irradiated in a first step, then homogenized to form reservoir(s) having a uniform ^{26}Al/^{27}Al.

We restrict here the discussion to the consequence of the present data on the maximum ^{26}Al production yields obtained in a solid target of chondritic (solar) composition.

In Figs. 7–9, we report all proton, α and ^{3}He induced reactions leading to ^{26}Al from neighboring target nuclei. All

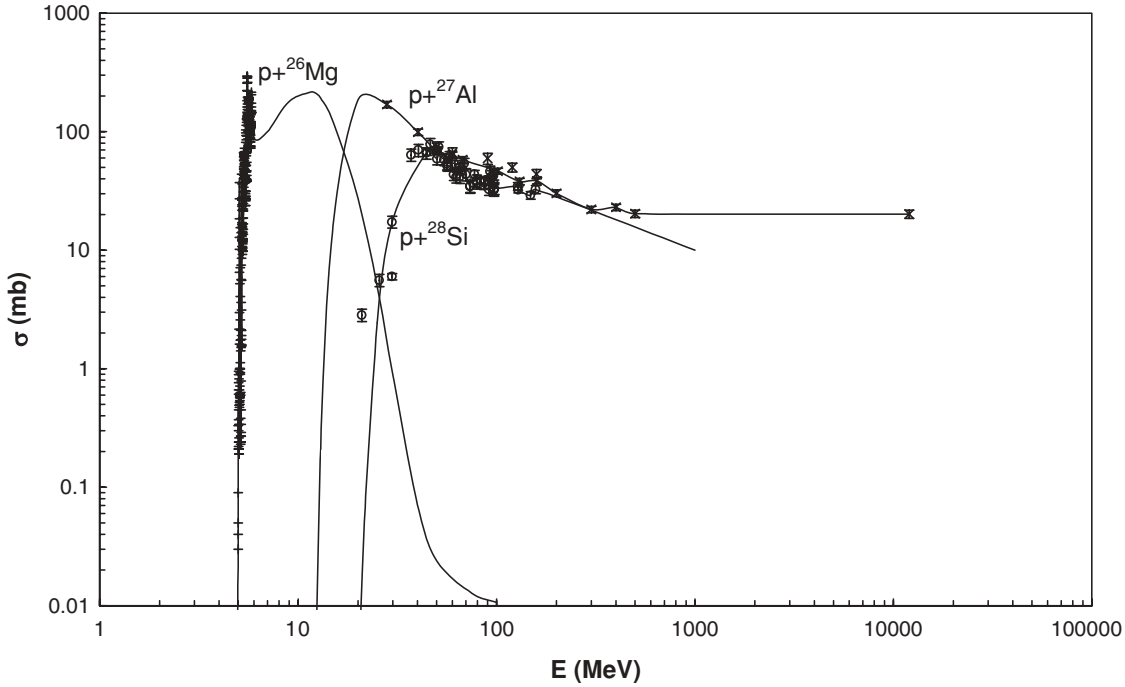

FIG. 7. Cross section for proton induced ^{26}Al obtained with TALYS code [41]. The data are from [43–46].

the excitation functions have been calculated using the TALYS code [41]. For proton-induced reactions we use the available data [43–46].

We considered differential flux of accelerated particles with a power law form:

$$\Phi_j(E, s) = K \times E^{-s}, \tag{1}$$

where s is the spectral index and K the normalization factor.

Detailed studies of modern sun flares indicate spectral indexes varying from hard ($s = 2.5$) to very soft ($s = 5$) spectrum.

Still, considering spectra with spectral index superior to 4 raises a critical energetic issue as the total kinetic energy in nonthermal particles, when integrated over the total irradiation period (about 3 Myr), reaches a value comparable to the total gravitational energy of the sun (3×10^{48} ergs) [47]. Therefore, we restricted the present study to $s = 2.5$–4.

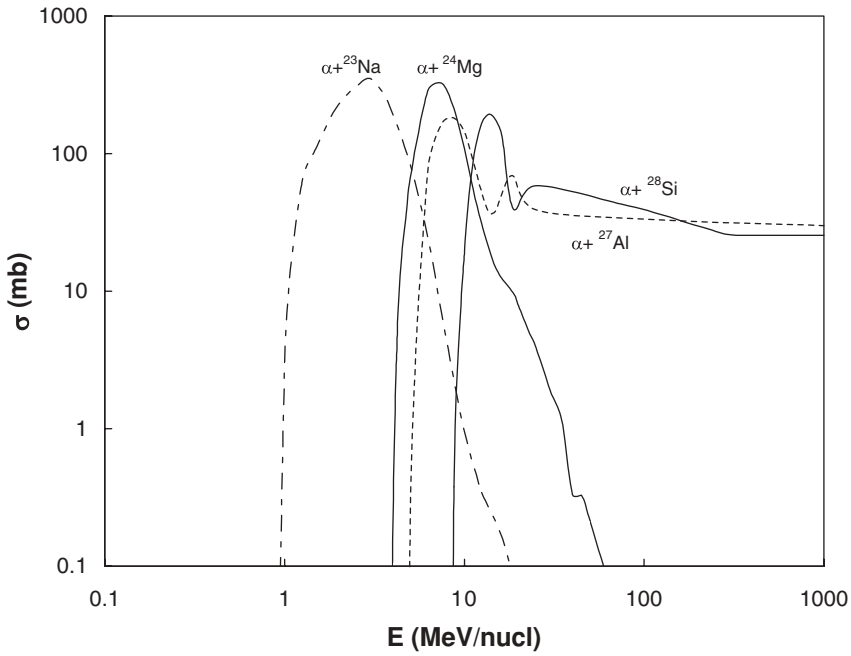

FIG. 8. Cross section for α-induced ^{26}Al obtained with TALYS code [41].

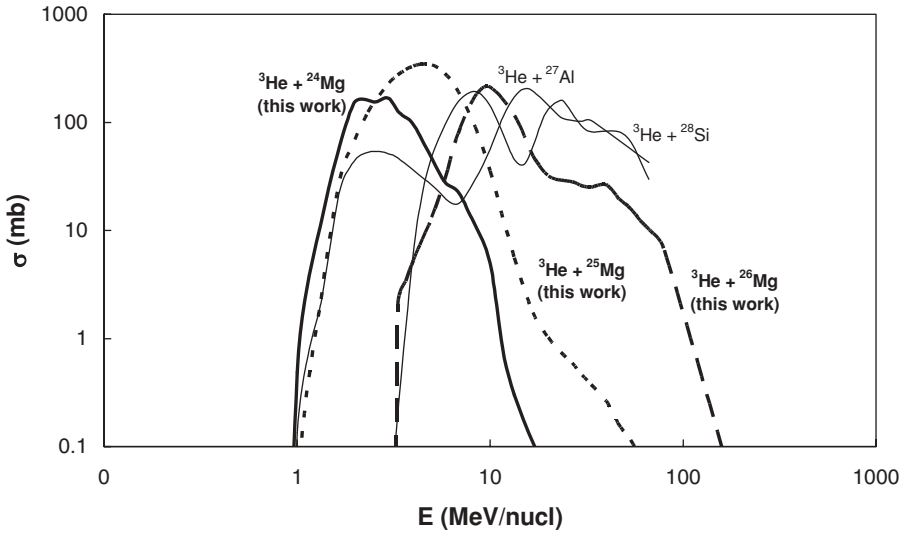

FIG. 9. Cross section for ^{3}He-induced ^{26}Al obtained with TALYS code [41].

We calculated the yields of the different reactions as

$$Q_{ij}(s) = n_i \int_0^\infty \Phi_j(E,s)dE \int_E^\infty \frac{\sigma_{ij}(E')}{\left(\frac{dE}{d\ell}\right)_j(E')}dE', \quad (2)$$

where n_i is the target abundance in atoms/g, $\Phi(E)$ is the normalized flux of particles of type j, σ_{ij} the reaction cross section, $dE/d\ell(E)$ is the energy loss rate in the target expressed in (MeV/nucleon) cm^{-1}. We calculated the energy losses using the SRIM code [39]. We considered a target of chondritic composition [48].

By analogy with impulsive flares of the modern Sun, we considered an abundance ratio of $\alpha/p = 0.1$ [49].

The ^{3}He abundance in impulsive solar flares exhibits highly variable values with ^{3}He/α ratios ranging from 0.1 up to extreme values of about 10 [50,51]. Still, most of the ^{3}He-rich flares have ^{3}He/$\alpha = 0.1$–1, with an average value of about 0.5 (see Fig. 2 in [50]).

In Fig. 10(a) and (b), we report the relative contribution to ^{26}Al production of proton, α and ^{3}He induced reactions for $s = 2.5$ and $s = 4$.

Considering ^{3}He/$\alpha = 0.5$, in the hard spectrum ($s = 2.5$) case ^{26}Al production is dominated by proton induced reactions, mainly on the abundant ^{28}Si target and ^{3}He induced reaction are negligible; while for $s = 4$, ^{26}Al is roughly equally produced by proton, α and ^{3}He induced reactions. In the latter case, the main production channels involve Mg target nuclei: ^{26}Mg(p, n), ^{24}Mg(α, pn), and ^{24}Mg(^{3}He, p), and the contribution of the two minor Mg isotopes stays marginal (<5%). It is worth noticing that, even in the most favorable case ($s = 4$), the ^{3}He contribution never exceeds about 30% of the total ^{26}Al production.

By contrast, if one considers ^{3}He/α ratios superior to 1, the proton-induced reactions still contribute at least 40% of the total yield in the $s = 2.5$ case (see Fig. 10(a)) while the ^{3}He-induced reactions largely dominate in the $s = 4$ case. The persistence of the p-induced reactions (even at large ^{3}He/α ratios) in the $s = 2.5$ case, is due to the contribution of the high energy tail of the ^{28}Si(p, $2pn$) cross section.

The occurrence of large ^{3}He fluxes in the early solar system remains unknown. If large amounts of ^{3}He have been accelerated by the young sun then indeed the production of ^{26}Al nuclei would have been dominated by the ^{24}Mg(^{3}He, p) reaction.

In Fig. 11, we report the yields expressed in terms of ^{26}Al nuclei produced per erg of accelerated particles above 1 MeV/nucleon for $s = 2.5$, 3, and 4.

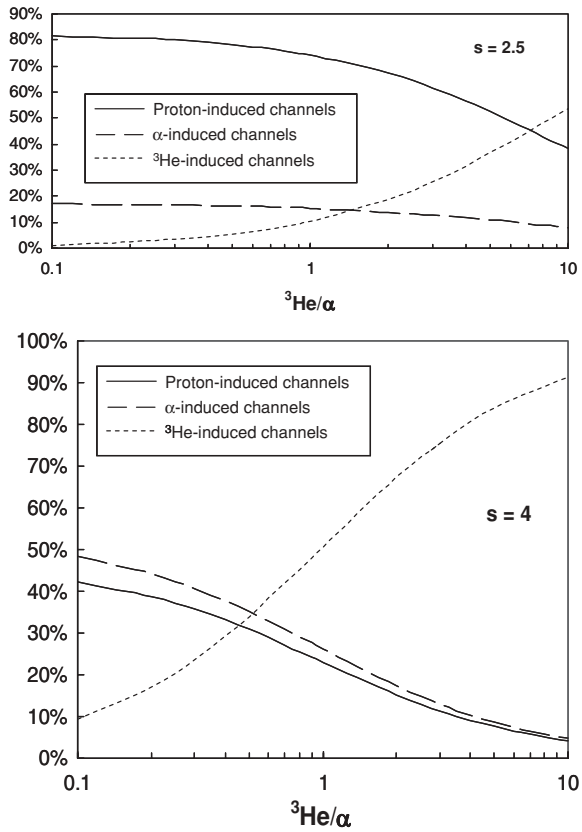

FIG. 10. Relative contribution of proton, α, and ^{3}He-induced reactions to ^{26}Al production (top $s = 2.5$, bottom $s = 4$).

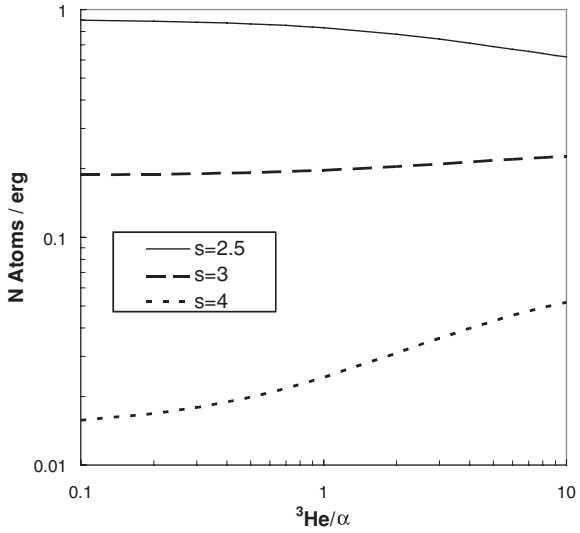

FIG. 11. ^{26}Al thick target yields Y in atoms/erg (for particles accelerated above 1 MeV nucl^{-1}). The accelerated particle spectra are power law $dE/dN = E^{-s}$ and we considered $\alpha/p = 0.1$. The target is of solar composition Na = 0.51 wt%, Mg = 9.74 wt%, Al = 0.86 wt%, Si = 10 wt%.

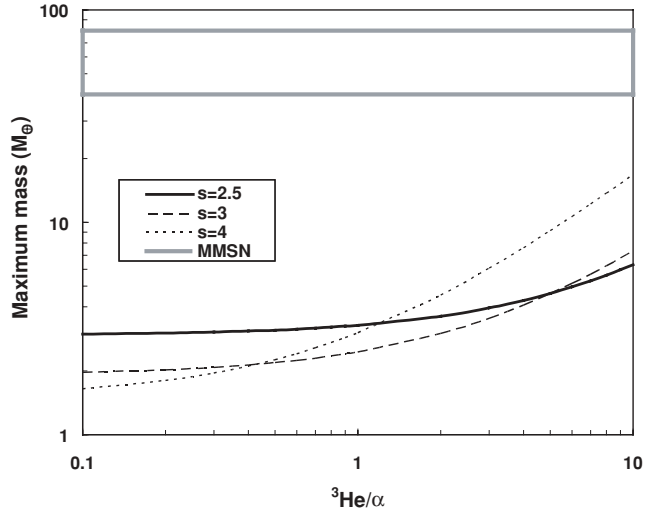

FIG. 12. Maximum mass (in Earth mass units) of chondritic material bearing irradiation-produced SLRs at their canonical abundance value, M^{max}, as a function of ^{3}He/α and spectral index of the accelerated particle energy spectrum. The SLR production is calculated for a solid target of chondritic composition [48] and normalized to a kinetic energy $E^{10MeV} = 4.3 \times 10^{43}$ ergs (see text). MMSN: the rocky component of the minimum mass solar nebula (see text and [52]).

In the $s = 4$ case, one can see a clear gain going from ^{3}He/$\alpha = 0.1$ to 10 due to the contribution of the ^{24}Mg(^{3}He, p) reaction. Nevertheless, the yields obtained remain more than an order of magnitude lower than the one obtained in the $s = 2.5$ case.

Taking the average ^{3}He/$\alpha = 0.5$, the yield varies between 2×10^{-2} and 8.6×10^{-1} ^{26}Al/erg for $s = 4$ and 2.5, respectively. The efficiency of production is larger for hard spectra as it benefits from the ^{28}Si(p, $2pn$) high energy tail.

Still the possibility to actually produce by irradiation a large amount of ^{26}Al in the early solar system raises severe difficulties.

The first difficulty deals with the total number of ^{26}Al produced compared to the planetary reservoir. Taking the yields from Fig. 11, one can compute an upper limit on the total number of ^{26}Al nuclei that can be synthesized over the entire irradiation episode. Using energetic constraints obtained from X-ray observations of young stellar objects [53], the total kinetic energy available in protons >10 MeV during the entire irradiation period is $E_p(>10\,\mathrm{MeV}) = 4.3 \times 10^{43}$ erg [18,47]. From the yields shown in Fig. 11, one can compute the maximum number of ^{26}Al, N ^{26}Al, that can be produced in the early solar system. For ^{3}He/$\alpha = 0.5$, N ^{26}Al depends only slightly on the spectral index, N ^{26}Al $= 1.8 \times 10^{44}$ for $s = 2.5$ and 1.3×10^{44} for $s = 4$.

From N ^{26}Al, one can infer the mass of the rocky reservoir of chondritic composition ([^{27}Al] = 0.86 wt%) having the canonical ^{26}Al/^{27}Al $= 5 \times 10^{-5}$, hereafter referred as M^{max}. The evolution as a function of ^{3}He/α of such reservoirs, expressed in terms of Earth Mass ($M_\oplus = 5.9 \times 10^{27}$ g) is reported on Fig. 12.

The inferred mass can be compared to the mass of rocks that actually survived stellar accretion to form the planets, that is 40–80 $M_\oplus$ (see [47] and references therein). The latter is hereafter referred as the minimum mass solar nebula (MMSN). For ^{3}He/α ranging from 0.1 to 1, M^{max} ranges from 1–2 $M_\oplus$, that is more than a factor of 10 lower than the MMSN. This demonstrates that, if one considers the ^{3}He/α ratios currently reported in ^{3}He-rich impulsive flares in the modern sun, it is not possible to produce enough ^{26}Al to account for a homogeneous distribution of this extinct nucleus over a reservoir comparable to the MMSN [47]. If one considers unusually high ^{3}He/α ratios (^{3}He/α = 1–10), it may be possible to produce enough ^{26}Al (essentially via the reaction on ^{24}Mg) to account for a reservoir of M^{max} of $\sim$10 $M_\oplus$ (for $s = 4$). This M^{max} is still significantly lower than the MMSN. Moreover, this higher M^{max} is not due to a more efficient production of ^{26}Al (see Fig. 11) but to the fact that this extreme scenario ($s = 4$,^{3}He/$\alpha = 10$) implicitly assumes that more energy is present in the non-thermal particles. The total energy in particles above 1 MeV/nucleon is 1.8×10^{46} erg, that is already about 1% of the total gravitational energy of the sun. Such a high value seems hard to imagine as an even much greater energy must be present in the particle spectrum below 1 MeV/nucleon [26].

A second difficulty concerns the irradiation scenario itself. The calculation of ^{26}Al/^{27}Al within a given irradiated solid requires a numerical simulation that should include the finite size of the target and the possibility for the recoiling ^{26}Al to actually escape from the target. Such a calculation exceeds the scope of the present paper. It is worth noting that, especially in the hard spectrum case ($s = 2.5$) the size of the target represents a severe issue, since for sizes below 0.1 cm the yield will be significantly reduced due to escape of the high energy part of the spectrum. By contrast, considering targets with sizes superior to a centimetre, the ^{26}Al produced will be too diluted to reach the canonical ratio.

Taking the yields indicated on Fig. 11 at ^{3}He/$\alpha = 0.5$ and assuming a 1 cm^3 target, the total particle fluence necessary to achieve the canonical ratio ranges from 1.4×10^{20} to 4.1×10^{20} protons ($E > 10$ MeV) cm^{-2} for $s = 4$ and 2.5, respectively. Such fluence is high and raises potentially severe problems to any irradiation scenario for producing ^{26}Al.

If one considers the irradiation of individual solids at large distance from the proto-Sun (1–3 AU) with fluxes about 10^5 times that observed in the modern Sun (i.e., $\Phi_p^{10\mathrm{MeV}} \sim 10^7 \mathrm{cm}^{-2}\mathrm{s}^{-1}$), in the $s = 4$ case it is barely possible to reach $^{26}\mathrm{Al}/^{27}\mathrm{Al} = 4 \times 10^{-5}$ ratio (saturation value) after a very long irradiation time $T_{\mathrm{irr}}^{\mathrm{ind}} > 3$ Myr. In the more favorable $s = 2.5$ case, the canonical $^{26}\mathrm{Al}/^{27}\mathrm{Al} = 5 \times 10^{-5}$ can be achieved after $T_{\mathrm{irr}}^{\mathrm{ind}} \sim 0.6$ Myr. This would require the irradiation of a reservoir of mm to cm-sized dust particles for a long period before this reservoir can eventually aggregate to form planetesimals. This would imply that the material that formed the planets of the inner solar system stayed for about a Myr in dust form at a few AU from the sun before being quickly accreted. Moreover, as emphasized by [17] the irradiation of solid targets at long distance from the nascent star is strongly reduced by the shielding of surrounding gas. For all these reasons, it is not conceivable to produce the early solar system ^{26}Al abundance ratio by irradiation of solid (or gas) targets at long distance from the star.

In the alternative scenario proposed by the x-wind model, the bare solids endure an intense irradiation episode at close distance (<0.1 AU) [17,30]. The instantaneous fluxes considered within such approaches are much higher $\Phi_p^{10\,\mathrm{MeV}} \sim 2 \times 10^{10}$ cm^{-2} s^{-1} [30]. Within such conditions, a canonical $^{26}\mathrm{Al}/^{27}\mathrm{Al}$ ratio can indeed be achieved within a few centuries for cm-sized (within decades for mm-sized) targets. We note that these values are roughly in agreement with the hypothesized residence time of the proto-CAIs in the reconnection ring [21,54].

Still, the total particle fluence received by the target in this scenario would then be extremely high since the particle fluxes are normalized at 10 MeV/nucleon, but their behavior must somehow be extended down to low energy. Most of the cross sections have their maximum between 1 and 10 MeV/nucleon and comprehensive studies of impulsive flares showed that the vast majority of the nonthermal particle kinetic energy lies below 1 MeV/nucleon-1 (i.e., below the nuclear reaction thresholds) [26,55]. Reames *et al.* [26] showed that, in impulsive flares, the particle fluxes increase with decreasing energy down to ∼0.02 MeV/nucleon, with an average spectral index $s \sim 2.5$ in the ∼0.02–1 MeV/nucleon energy range.

Let us consider an idealistic differential spectrum having different spectral indexes depending on the energy range, with s ranging from 2.5 to 4 for $E > 1$ MeV/nucleon, $s = 2.5$ for $0.02 < E < 1$ MeV/nucleon and a flat behavior ($s = 0$) below 0.02 MeV/nucleon. Assuming such a spectrum, the total fluence required for a 1 cm^3 target to reach the canonical ratio would range from 2×10^{24} particles/cm^2 for $s = 2.5$ up to 3.3×10^{26} particles/cm^2 for $s = 4$. We note that in the $s = 4$ case, the instantaneous flux $\Phi_p^{10\mathrm{MeV}} \sim 2 \times 10^{10}$ cm^{-2} s^{-1} corresponds, considering the complete spectrum described above, to a flux of 1.7×10^{16} particle cm^{-2}s^{-1}. Such a flux exceeds by an order of magnitude the typical atomic surface density (2×10^{15} at/cm^2) and the average energy deposition would amount to $E = 2.4 \times 10^{15}$ erg cm^{-2}s^{-1} with a corresponding temperature of equilibrium ($E = \sigma T^4$, where σ is the Stefan-Boltzmann constant), $T \sim 2500$ K. Shu *et al.* 2001 [54] suggested that the proto-CAIs must have experienced repeated episodes of melting-condensing sequences during their passage in the irradiation zone. However, we note that under such average bombardment conditions the proto-CAI target cannot survive as a solid during the typical duration of a flare (3 h–3 d) [56].

For all these reasons, only minute amounts of ^{26}Al can be achieved by irradiation and, except if one demonstrates that this radionucleus was actually only present in an extremely restricted ESS reservoir, its origin should be searched for in stellar nucleosynthetic event(s) that occurred within the local environment (i.e., within a few parsecs and Myr) of the solar system birth. However an external origin also faces difficulties that include the existence of a population of primitive refractory solids that exhibit a low, if not zero, initial ^{26}Al (see [17]). Recently, it has been emphasized that the probability to contaminate the protoplanetary disk with freshly nucleosynthesized isotopes from a unique massive star that exploded at the vicinity of the ESS is rather low [57].

As a result, the nucleosynthetic origin (if unique?) of the ^{26}Al in the ESS is still a challenge to theory. In that perspective, we emphasize that the real issue is not the mere presence of live ^{26}Al nuclei in the ESS but the fact that the inferred $^{26}\mathrm{Al}/^{27}\mathrm{Al}$ has been so far considered to be incompatible with theoretical expectations for the protosolar nebula. Still, that latter statement should be taken cautiously. Indeed, using the germanium spectrometer telescope (SPI) onboard the INTERGRAL γ-ray observatory of the European Space agency, Diehl *et al.* (2006) reported new spectra of celestial ^{26}Al emission [58]. Taking the total 1.8 MeV γ-ray flux, Diehl *et al.* inferred a present day galactic ^{26}Al equilibrium mass of (2.8 ± 0.8) M$_\odot$ and a corresponding average $^{26}\mathrm{Al}/^{27}\mathrm{Al} = 0.84 \times 10^{-5}$ [58]. The relative uncertainty on the latter value is, at least, about 30%, so that the upper limit is only about a factor of 5 below the ESS value. Given the uncertainties on various parameters such as the mass of both ^{26}Al and ^{27}Al in the ISM 4.6 Gyr ago, and their spatial heterogeneities, it might be that, locally, molecular cloud cores may arise with $^{26}\mathrm{Al}/^{27}\mathrm{Al}$ superior to 5×10^{-5}, allowing the development of a protosolar nebula with a bulk $^{26}\mathrm{Al}/^{27}\mathrm{Al}$ compatible with the value recorded in primitive solar system rocks [59].

IV. CONCLUSION

We measured the cross section for ^{26}Al production by ^{3}He reactions on Mg target nuclei. The main production channel, ^{24}Mg(^{3}He, p)^{26}Al, has been measured by means of accelerator mass spectrometry over the 6–25 MeV energy range and by γ-ray spectroscopy from 3 to 36 MeV. The excitation function is found to be well reproduced by the

numerical reaction code TALYS. We note that recent preliminary data on different ^{3}He-induced reactions leading to ^{26}Al, ^{36}Cl, and ^{41}Ca [60] seems to confirm the accuracy of the TALYS code. The ^{25}Mg and ^{26}Mg contributions to the ^{26}Al first 3^{+} excited state have also been evaluated by means of γ-ray spectroscopy and their total contribution to the long lived 5^{+} ground state have been extrapolated using the TALYS code. The total ^{26}Al production is found to be reduced by a factor of two compared to previous work [17,30]. We calculated the relative contribution of all reactions leading to ^{26}Al production from Mg, Al, and Si targets. If the particles accelerated in the early solar system have chemical composition comparable to the one currently reported in modern solar impulsive flares, the relative contribution of ^{3}He induced reactions represents, at the maximum, about one-third of the ^{26}Al production. We emphasize that the total fluence necessary to reach the canonical ^{26}Al abundance in cm-sized targets is extremely high and not compatible with irradiation of solids at asteroidal distances from the nascent sun. Moreover, we show that irradiation by soft particle spectra ($s = 4$) such as currently observed in impulsive solar flares, raises severe target issues and it is not clear that the proto-CAI can survive the inferred particle fluxes. Finally, we demonstrate that it is not possible to produce by irradiation a large reservoir of rocks having $^{26}\mathrm{Al}/^{27}\mathrm{Al} = 5 \times 10^{-5}$ and the origin of this radioactivity in the primitive meteorites is most probably external to the solar system itself.

ACKNOWLEDGMENTS

We would like to thank the operator crew of the Orsay Tandem accelerator for their engagement in the preparation of the experiment and M.-A. Saettel of the IPHC-Strasbourg (former IRES) for the manufacturing of the targets. Tandetron operation was supported by the IN2P3 and INSU divisions of the CNRS.

[1] T. Lee, D. A. Papanastassiou, and G. J. Wasserburg, Geophys. Res. Lett. **3**, 109 (1976).
[2] G. J. MacPherson, A. M. Davis, and E. K. Zinner, Meteoritics **30**, 365 (1995).
[3] M. Bizzarro, J. A. Baker, and H. Haack, Nature (London) **431**, 275 (2004).
[4] E. D. Young, J. I. Simon, A. Galy, S. S. Russell, E. Tonui, and O. Lovera, Science **308**, 223 (2005).
[5] Y. Amelin, A. N. Krot, I. D. Hutcheon, and A. A. Ulyanov, Science **297**, 1678 (2002).
[6] G. J. Wasserburg, M. Busso, R. Gallino, and K. M. Nollett, Nucl. Phys. **A777**, 5 (2006).
[7] E. Zinner, Science **300**, 265 (2003).
[8] B. S. Meyer and D. D. Clayton, Space Sci. Rev. **92**, 133 (2000).
[9] J. N. Goswami and H. A. T. Vanhala, in *Protostars and Planets IV*, edited by V. Mannings, A. P. Boss, and S. S. Russell, (University of Arizona Press, Tucson, 2000), p. 963.
[10] M. Arnould, G. Paulus, and G. Meynet, Astron. Astrophys. **321**, 452 (1997).
[11] G. J. Wasserburg, M. Busso, R. Gallino, and C. M. Raiteri, Astrophys. J. **424**, 412 (1994).
[12] G. J. Wasserburg, R. Gallino, and M. Busso, Astrophys. J. Lett. **500**, L189 (1998).
[13] S. Mostefaoui, G. W. Lugmair, P. Hoppe, and A. El Goresy, New Astron. Rev. **48**, 155 (2004).
[14] S. E. Woosley and T. A. Weaver, Astrophys. J. Suppl. **101**, 181 (1995).
[15] T. Rauscher, A. Heger, R. D. Hoffman, and S. E. Woosley, Astrophys. J. **576**, 323 (2002).
[16] M. Limongi and A. Chieffi, Astrophys. J. **592**, 404 (2003).
[17] T. Lee, F. H. Shu, H. Shang, A. E. Glassgold, and K. E. Rehm, Astrophys. J. **506**, 898 (1998).
[18] W. A. Fowler, Science **135**, 1037 (1962).
[19] J. N. Goswami, K. K. Marhas, and S. Sahijpal, Astrophys. J. **549**, 1151 (2001).
[20] I. Leya, A. N. Halliday, and R. Wieler, Astrophys. J. **594**, 605 (2003).
[21] M. Gounelle, F. H. Shu, H. Shang, A. E. Glassgold, K. E. Rehm, and T. Lee, Astrophys. J. **548**, 1051 (2001).
[22] E. D. Feigelson, G. P. Garmire, and S. H. Pravdo, Astrophys. J. **572**, 335 (2002).
[23] F. H. Shu, H. Shang, and T. Lee, Science **271**, 1545 (1996).
[24] F. H. Shu, H. Shang, A. E. Glassgold, and T. Lee, Science **277**, 1475 (1997).
[25] D. V. Reames, in *High Energy Solar Physics*, edited by R. Ramaty, N. Mandzhavidze, and X. Hua, AIP Conf. Proc. No. 374 (AIP, Woodbury, NY, 1996), p. 35.
[26] D. V. Reames, L. M. Barbier, T. T. von Rosenvinge, G. M. Mason, J. E. Mazur, and J. R. Dwyer, Astrophys. J. **483**, 515 (1997).
[27] N. Mandzhavidze, R. Ramaty, and B. Kozlovsky, Astrophys. J. **518**, 918 (1999).
[28] G. Srinivasan, A. A. Ulyanov, and J. N. Goswami, Astrophys. J. Lett. **431**, L67 (1994).
[29] G. Srinivasan, S. Sahijpal, A. A. Ulyanov, and J. N. Goswami, Geochim. Cosmochim. Acta **60**, 1823 (1996).
[30] M. Gounelle, F. H. Shu, H. Shang, A. E. Glassgold, K. E. Rehm, and T. Lee, Astrophys. J. **640**, 1163 (2006).
[31] K. D. McKeegan, M. Chaussidon, and F. Robert, Science **289**, 1334 (2000).
[32] A. Gavron, Phys. Rev. C **21**, 230 (1980).
[33] R. R. Betts, H. T. Fortune, and D. J. Pullen, Phys. Rev. C **6**, 957 (1972).
[34] R. B. Firestone and V. S. Shirley, *Table of Isotopes*, 8th ed., Vol. II (Wiley, New York, 1996).
[35] V. Tatischeff *et al.*, Phys. Rev. C **68**, 025804 (2003).
[36] G. M. Raisbeck, F. Yiou, C. Eymas, and J. Lestringuez, Nucl. Instrum. Methods B **172**, 170 (2000).
[37] P. J. Nolan, F. A. Beck, and D. B. Fossan, Annu. Rev. Nucl. Part. Sci. **44**, 561 (1994).
[38] X. Grave *et al.*, 14th IEEE-NPSS Real Time Conference, 2005, p. 65.
[39] J. F. Ziegler, Nucl. Instrum. Methods B **219**, 1027 (2004), see also URL: http://www.srim.org/.
[40] A. J. Ferguson, *Angular Correlation Methods in Gamma-Ray Spectroscopy* (North-Holland, Amsterdam, 1965).
[41] A. J. Koning, S. Hilaire, and M. C. Duijvestijn, AIP Conf. Proc. **769**, 1154 (2005).

[42] M. Gounelle and S. S. Russell, Geochim. Cosmochim. Acta **69**, 3129 (2005).
[43] R. J. Schneider, J. M. Sisterson, A. M. Koehler, J. Klein, and R. Middleton, Nucl. Instrum. Methods B **29**, 271 (1987).
[44] J. M. Sisterson, K. Kim, A. Beverding, P. A. J. Englert, M. W. Caffee, J. Vincent, C. Castaneda, and R. C. Reedy, in *Application of Accelerators in Research and Industry*, edited by J. L. Duggan and I. L. Morgan, AIP Conf. Proc. No. 392 (AIP, New York, 1997), p. 811.
[45] S. Shibata, M. Imamura, H. Nagai, K. Kobayashi, K. Sakamoto, M. Furukawa, and I. Fujiwara, Phys. Rev. C **48**, 2617 (1993).
[46] R. T. Skelton, R. W. Kavanagh, and D. G. Sargood, Phys. Rev. C **35**, 45 (1987).
[47] J. Duprat and V. Tatischeff, Astrophys. J. Lett. **671**, L69 (2007).
[48] K. Lodders, Astrophys. J. **591**, 1220 (2003).
[49] D. V. Reames, Space Sci. Rev. **90**, 413 (1999).
[50] D. V. Reames, J. P. Meyer, and T. T. von Rosenvinge, Astrophys. J. Suppl. Ser. **90**, 649 (1994).
[51] G. M. Mason *et al*., Astrophys. J. **574**, 1039 (2002).
[52] S. P. Ruden, in *The Origin of Stars and Planetary Systems*, edited by C. J. Lada and N. D. Kylafis, NATO ASI Ser. C, 540 (Kluwer, Dordrecht, 1999), p. 643.
[53] T. Preibisch and E. D. Feigelson, Astrophys. J. Suppl. Ser. **160**, 390 (2005).
[54] F. H. Shu, S. Shang, M. Gounelle, A. E. Glassgold, and T. Lee, Astrophys. J. **548**, 1029 (2001).
[55] G. H. Share, R. J. Murphy, and E. K. Newton, Sol. Phys. **201**, 191 (2001).
[56] S. J. Wolk, F. R. Harnden Jr., E. Flaccomio, G. Micela, F. Favata, H. Shang, and E. D. Feigelson, Astrophys. J. Suppl. Ser. **160**, 423 (2005).
[57] M. Gounelle and A. Meibom, Astrophys. J. **680**, 781 (2008).
[58] R. Diehl *et al*., Nature (London) **439**, 45 (2006).
[59] M. Gounelle *et al*., Astrophys. J., submitted (2008).
[60] M. W. Caffee, T. Faestermann, R. Hertenberger, G. F. Herzog, G. Korschinek, I. Leya, R. C. Reedy, and J. M. Sisterson, Proc. Lunar Sci. Conf., **39**, 1258 (2008).